

RESEARCH ARTICLE | AUGUST 30 2023

Low temperature epitaxial growth of Cantor-nitride thin films by magnetic field assisted magnetron sputtering ^{EP}

Special Collection: [Celebrating the Achievements and Life of Joe Greene](#)

Smita G. Rao ^{ID}; Pascal Manuel Illgner; Robert Boyd ^{ID}; Gyula Nagy ^{ID}; Philippe Djemia ^{ID}; Daniel Primetzhofer ^{ID}; Ivan Petrov ^{ID}; Arnaud le Febvrier ^{ID}; Per Eklund ^{ID}



J. Vac. Sci. Technol. A 41, 053415 (2023)

<https://doi.org/10.1116/6.0002947>



CrossMark



Instruments for Advanced Science

- Knowledge
- Experience
- Expertise

Click to view our product catalogue

Contact Hiden Analytical for further details:

www.HidenAnalytical.com

info@hiden.co.uk

Gas Analysis

- dynamic measurement of reaction gas streams
- catalysis and thermal analysis
- molecular beam studies
- dissolved species probes
- fermentation, environmental and ecological studies

Surface Science

- UHV TPD
- SIMS
- end point detection in ion beam etch
- elemental imaging - surface mapping

Plasma Diagnostics

- plasma source characterization
- etch and deposition process reaction kinetic studies
- analysis of neutral and radical species

Vacuum Analysis

- partial pressure measurement and control of process gases
- reactive sputter process control
- vacuum diagnostics
- vacuum coating process monitoring









Low temperature epitaxial growth of Cantor-nitride thin films by magnetic field assisted magnetron sputtering

Cite as: J. Vac. Sci. Technol. A 41, 053415 (2023); doi: 10.1116/6.0002947

Submitted: 5 July 2023 · Accepted: 8 August 2023 ·

Published Online: 30 August 2023



Smita G. Rao,¹  Pascal Manuel Illgner,¹ Robert Boyd,²  Gyula Nagy,³  Philippe Djemia,⁴ 
Daniel Primetzhofer,³  Ivan Petrov,^{1,5}  Arnaud le Febvrier,^{1,a)}  and Per Eklund¹ 

AFFILIATIONS

¹Department of Physics, Chemistry, and Biology (IFM), Thin Film Physics Division, Linköping University, Linköping 58183, Sweden

²Department of Physics, Chemistry, and Biology (IFM), Plasma and Coatings Physics Division, Linköping University, Linköping 58183, Sweden

³Department of Physics and Astronomy, Uppsala University, Lägerhyddsvägen 1, Uppsala S-75120, Sweden

⁴Université Sorbonne Paris Nord, Alliance Sorbonne Paris Cité, Laboratoire des Sciences des Procédés et des Matériaux, UPR 3407 CNRS, Villeteuse F-93430, France

⁵Materials Research Laboratory and Department of Materials Science, University of Illinois, Urbana, Illinois 61801

Note: This paper is part of the Special Topic Collection Celebrating the Achievements and Life of Joe Greene.

^{a)}Electronic mail: arnaud.le.febvrier@liu.se

ABSTRACT

Low-temperature epitaxial growth of multicomponent alloy-based thin films remains an outstanding challenge in materials science and is important for established fundamental properties of these complex materials. Here, Cantor nitride (CrMnFeCoNi)N thin films were epitaxially grown on MgO(100) substrates at low deposition temperature by magnetic-field-assisted dc-magnetron sputtering, a technique where a magnetic field is applied to steer the dense plasma to the substrate thereby influencing the flux of Ar-ions bombarding the film during growth. Without ion bombardment, the film displayed textured growth. As the ion flux was increased, the films exhibited epitaxial growth. The epitaxial relationship between film and substrate was found to be cube on cube (001)film||[(001)MgO, [100]film||[[100]MgO. The epitaxy was retained up to a thickness of approximately ~ 100 nm after which the growth becomes textured with a 002 out-of-plane orientation. The elastic constants determined by Brillouin inelastic light scattering were found to be $C_{11} = 320$ GPa, $C_{12} = 125$ GPa, and $C_{44} = 66$ GPa, from which the polycrystalline Young's modulus was calculated as 204 GPa and Poisson's ratio = 0.32, whereas available elastic properties still remained very scarce.

© 2023 Author(s). All article content, except where otherwise noted, is licensed under a Creative Commons Attribution (CC BY) license (<http://creativecommons.org/licenses/by/4.0/>). <https://doi.org/10.1116/6.0002947>

I. INTRODUCTION

The Cantor alloy (CrMnFeCoNi) has gained immense popularity since 2004 for its simple face centered cubic structure despite the complex elemental composition.¹ Its mechanical properties, such as low-temperature ductility and fracture toughness, have made the Cantor alloy an attractive candidate as structural materials.² While the bulk polycrystalline metallic alloy and its variants continue to attract experimental and theoretical interest,^{3–5} thin

films of the Cantor alloy are also of great interest. This is due to the possibility of broadening the compositional space available by the addition of light elements, such as carbon, nitrogen, and oxygen.^{6,7} Gaining a fundamental understanding of this material system could not only broaden the applications of Cantor alloy-based ceramics but also provide a solution for replacing existing coatings with a more economical alternative.

Here, we investigate the Cantor nitride. The difficulty with this material system is the lack of a fundamental understanding of

the material originating from the inconsistency in the growth morphology and texture between studies. Recent studies^{8–10} have begun elucidating the phase evolution of nitrogen containing multicomponent alloy thin films; however, a detailed understanding of Cantor alloy nitride layers is lacking.

These complexities can be reduced if the material system is studied as epitaxial films. For many decades, such studies have been carried out on binary and ternary nitrides, in order to understand the effect of vacancies and defects on the mechanical properties.^{8–11} Furthermore, the epitaxial growth of films allows determining direction-dependent properties either by measurements, modeling, simulation, or density function theory calculations.^{12–15}

In order to achieve epitaxial growth, most studies rely on high deposition temperatures above 700 °C, where the substrate heating provides enough thermal energy to the adatom to occupy the lattice positions similar to those of the substrate.^{16–18} High temperature magnetron sputtering may not be the best approach for specific systems where the temperature can be a limiting factor and can lead to degradation of the material. In the present case of the Cantor nitride, the material system displays an NaCl B1 structure only at low deposition temperatures (200–300 °C).¹⁹ This would make epitaxial growth impossible using conventional magnetron sputtering at high deposition temperatures.

Recently, techniques, such as high power impulse magnetron sputtering (HiPIMS), have been used to grow epitaxial HfN films on MgO at low temperatures.²⁰ The thermal energy provided by substrate heating is replaced by kinetic energy through energy transfer from an incoming flux of metal ions. HiPIMS, however, is a complex technique to use while dealing with multicomponent materials, where complications rise with multiple ionization levels on different elements. In such a case, we look back on to an older technique of magnetron sputtering known as magnetic-field-assisted magnetron sputtering.²¹ Here, a solenoid coil placed around the substrate produces a magnetic field, which aids in condensing the plasma toward the substrate, thereby increasing the Ar-ion flux at the substrate. The Ar-ion energy, in turn, is controlled by the applied bias voltage to substrate. Previous studies on the (CrFeCoNi)N system showed that high energy Ar-ion bombardment at low deposition temperature can lead to amorphization.²² On the other hand, low-energy ion bombardment during film growth is known alter nucleation kinetics as well as provide a gentle etching effect to the growing film and has been well established in the low-temperature epitaxial growth of binary nitrides.^{23–28}

Taking into consideration all these factors, magnetic-field-assisted magnetron sputtering was employed for low-temperature epitaxial growth of Cantor nitrides. The study not only proves that it is possible to grow single phase Cantor nitrides following the results published in Ref. 19 but also goes on to establish deposition parameters/conditions required for epitaxial growth as well as fundamental mechanical properties. The results presented in the study are aimed to be of use for future research toward understanding Cantor alloy-based ceramic thin films.

II. EXPERIMENTAL METHODS

(CrMnFeCoNi)N thin films were grown on 10 × 10 mm² MgO (100) substrates by magnetic-field-assisted magnetron sputtering.

Prior to deposition, the substrates were cleaned with a Hellmanex®II, 2 vol. % diluted solution followed by de-ionized water, acetone, and ethanol.²⁹ The wet-cleaned substrates were then annealed at 800 °C for 1 h inside the deposition chamber to atomically reconstruct the surface. The substrates were cooled down to room-temperature before deposition.

The films were grown using a compound target of composition Cr₂₀Mn₂₀Fe₂₀Co₂₀Ni₂₀ provided by Plansee, Composite Materials GmbH (target thickness—3 mm, 50.8 mm diameter). The deposition chamber consists of four magnetrons that are approximately 13 cm below the substrate holder. A magnetic field is created around the substrate with the help of a solenoid coil. Details on the ultrahigh vacuum sputtering system are described elsewhere.³⁰ The base pressure was 3 × 10^{−7} Pa. Depositions were carried out in an Ar + N₂ atmosphere (working pressure, 0.53 Pa), where the relative nitrogen gas flow (F_{N_2}) = 80% [$F_{N_2} = f_{N_2} / (f_{N_2} + f_{Ar})$, f_{N_2} is the nitrogen partial flow, and f_{Ar} is the argon partial flow].

Langmuir and flat probes were used to determine the plasma potential, floating potential and ion fluxes on the substrates.³¹

A PANalytical X'Pert PRO diffractometer was used to obtain θ -2 θ x-ray diffraction patterns in Bragg–Brentano configuration. Reciprocal space maps (RSM) and x-ray reflectivity measurements (XRR) were obtained using a PANalytical Empyrean x-ray diffractometer. Both instruments were operated using Cu-K α radiation ($\lambda = 1.54060$ Å) at a voltage of 45 kV and current of 40 mA. The XRR spectra were analyzed using the PANalytical X'pert reflectivity software.

A scanning electron microscope (SEM, ZEISS GeminiSEM 650) operated with an acceleration voltage of 1 kV and in-lens detector was used to observe the surface as well as cross-sectional morphology.

The composition of the films was determined by a combination of ion beam analysis techniques. The nitrogen content relative to the cumulative metal content (N/metal) was obtained by time-of-flight elastic recoil detection analysis (ToF-ERDA). Particle induced x-ray emission (PIXE) was used to resolve the concentration of individual metals (Cr, Mn, Fe, Co, Ni). The areal density of the films was obtained by Rutherford backscattering spectrometry (RBS). Measurements were carried at the 5 MV NEC-5SDH-2 Pelletron Tandem accelerator of the Tandem Laboratory, Uppsala University, Sweden.³² ToF-ERDA measurements were carried out using a 36 MeV ¹²⁷I⁸⁺ beam. The beam incidence angle on the target was 67.5° with respect to the surface normal, while the ToF-telescope and the gas ionization chamber detector were placed at 45° relative to the incident beam direction. Depth profiles of the elemental composition were acquired from ToF-ERDA time and energy coincidence spectra with the POTKU 2.0 software package.³² PIXE and RBS measurements were carried out simultaneously using a beam of 2 MeV He⁺ primary ions with 5° incident angle between the beam and the sample normal. The x-ray and the back-scattered particle detection angle was 135° and 170°, respectively. The acquired PIXE spectra were fitted using the GUPIX code,³³ while the RBS spectra were processed using the SIMNRA software, version 7.03.³⁴

A Zeiss Neon 40 dual beam workstation was used to prepare electron transparent samples by focused ion beam milling. The

instrument was operated using 30 kV/2 nA Ga⁺ ion. The electron transparent cross sections were analyzed by (scanning) transmission electron microscopy [(S)TEM], and high resolution-TEM (HRTEM) using an FEI Tecnai G2 TF 20 UT instrument operated at 200 kV. STEM images were collected with the annular detector spanning the range 80–260 mrad.

Brillouin inelastic light scattering (BLS) was used in order to determine the sound velocities of surface acoustic waves (SAW), namely, Rayleigh and Sezawa surface waves traveling parallel to the film plane.^{8,35} Knowing the thickness (*t*) and the mass density (*ρ*), we were able to fit Brillouin spectra and provided the elastic constants of the Cantor nitride film.

The BLS setup consisted of a single-mode p-polarized YAG solid-laser laser ($\lambda = 532$ nm) with a power of 200 mW, which was focused on the film surface. Measurements were performed in the backscattering geometry at an incidence angle of $\theta = 65^\circ$, for two directions of propagation, along MgO [100] and [110] directions. The backscattered light was analyzed in the frequency domain with a Sandercock-type tandem (3 + 3 pass) Fabry–Pérot interferometer. The wave vector modulus of SAW is defined by $Q = 4\pi \sin(\theta)/\lambda$ and sound velocity by $V_{SAW} = f/2p/Q$, *f* being the Brillouin frequency of a SAW.

The self-consistent calculations—elasticity of multiphase aggregate (SC-EMA) software^{36–38} was used to calculate Young's modulus and Poisson's ratio for the polycrystalline cubic material.

III. RESULTS

A series of seven Cantor nitride, (CrMnFeCoNi)N, films were grown by reactive magnetron sputtering on MgO (100) substrates. Table I lists the extracted floating potential and ion flux values for each magnetic field estimated from the plasma characterization. Note here that the plasma characterization has been performed in the same condition as the film deposition (refer to Sec. II). The magnetic field at the substrate was increased from 0 to 8.5 mT. As the magnetic field is increased, the floating potential decreased from −5 to −16 V (see Fig. S1 in the supplementary material⁴⁸ for flat probe I–V characteristics). The plasma study also showed an increase in ion flux from $\sim 1.5 \times 10^{14} \text{ cm}^{-2} \text{ s}^{-1}$ when no magnetic field is applied to $9 \times 10^{14} \text{ cm}^{-2} \text{ s}^{-1}$ when the magnetic field is set at 8.5 mT (Ref. 22) (Table I). To maintain a low energy of the Ar-ions, the substrate bias was set at −20 V which corresponded to

an ion energy of ~ 20 eV. The plasma potential remained between 1 and 2 V. The deposition metal atom flux, calculated from the PIXE data, is 5.0×10^{14} metal atoms/cm²/s for all the films, irrespective of the applied magnetic field. Thus, the ion-to-metal flux ratio varies from ~ 0.3 to 1.8 in the range of magnetic fields studied.

The composition and density of the Cantor nitride films is shown in Table II. The nitrogen content reported for the series is intended for comparison between the sample and not for consideration as absolute values. ToF-ERDA measurements on the films reported an average of almost 60% metal and 40% nitrogen content in all the films with at most 1% of oxygen as the sole additional species detected (see Table II in the supplementary material⁴⁸ for more information). The density of the films measured by XRR increases from 6.20 to 6.72 g/cm³ with increasing magnetic field from 0 to 8.5 mT. The thickness of the films ranged between 400 and 460 nm.

Figure 1(a) shows the x-ray diffractograms of the Cantor nitride thin films grown by increasing the magnetic field from 0 to 8.5 mT at the substrate. Figure 1(b) shows the trend in full width at half maximum (FWHM) of the peak at $2\theta = 44.3^\circ$. The peaks marked with “*” indicate the MgO substrate peaks. The substrate peaks are observed at 2θ values of 43.0° and 93.9° . Only two other peaks at $2\theta = 44.3^\circ$ and 98.2° are observed and identified as the 200 and 400 reflections of a cubic material system, isostructure of an NaCl B1 structured material. As the magnetic field is increased the peak intensities increase with a decrease of the FWHM indicating an improvement in the crystal quality. The cell parameter of the films was calculated to be $4.08 \pm 0.02 \text{ \AA}$ irrespective of the increasing magnetic field.

Figure 2(a) shows the rocking curve measurements carried out on the 002 reflection of the NaCl B1 structured Cantor nitride thin films at an azimuth angle (ϕ) of 0° . As the magnetic field is increased from 0 to 8.5 mT, an increase in the peak intensity along with a decrease in the FWHM of the peaks is observed, implying a reduction of the mosaicity at higher magnetic fields. Similar trends in the intensity and FWHM are also observed in the θ - 2θ scans (Fig. 1) obtained in Bragg–Brentano setup.

Figure 2(b) shows the rocking curves of the 002 reflection obtained at $\phi = 90^\circ$. All the samples present the double peak feature.

TABLE II. Composition of Cantor nitride films obtained by PIXE/ToF-ERDA and density obtained by x-ray reflectivity, respectively.

Magnetic field (mT)	PIXE/ToF-ERDA composition analyses ($\pm 0.5\%$)						Density (XRR, g/cm ³)
	Cr	Mn	Fe	Co	Ni	N	
0	9.0	12.1	12.1	13.3	13.7	39.9	6.20
1.5	9.6	12.0	12.0	13.2	13.3	39.9	6.24
3.5	9.7	12.0	12.1	12.9	13.2	40.0	6.64
5.5	8.7	11.9	12.2	13.0	13.3	40.9	6.64
6.5	9.0	12.0	12.4	13.6	13.6	39.4	6.62
7.5	8.8	11.7	12.0	13.3	13.7	40.6	6.60
8.5	9.0	12.4	12.0	13.0	13.5	40.2	6.72

TABLE I. Floating potential and approximate ion flux at the substrate for increasing magnetic field.

Magnetic field (mT)	Floating potential (V)	Ion flux ($\times 10^{14} \text{ cm}^{-2} \text{ s}^{-1}$)
0	−5.02	1.5
1.5	−5.33	2.0
3.5	−8.09	5.0
5.5	−10.78	7.5
6.5	−13.29	8.0
7.5	−15.25	8.5
8.5	−16.18	9.0

12 February 2024 15:01:40

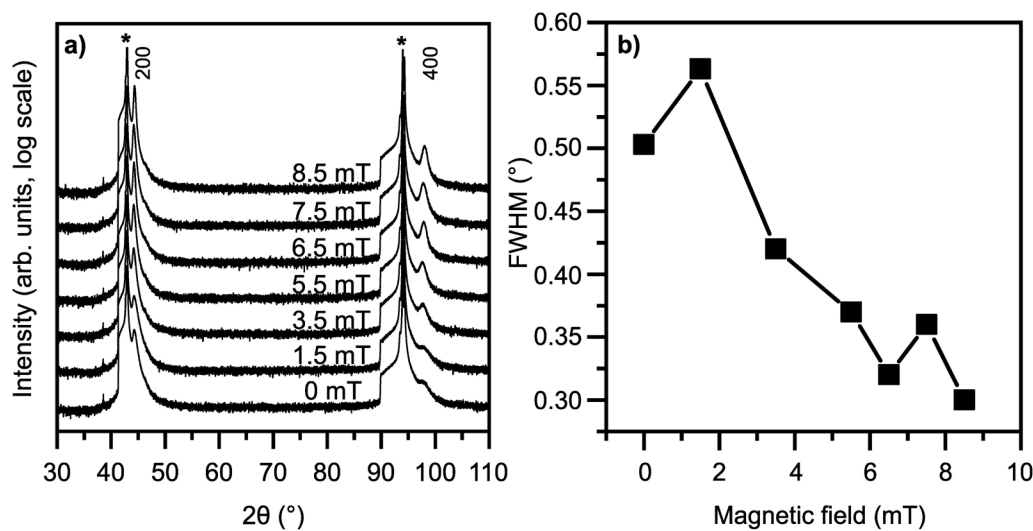


FIG. 1. (a) X-ray diffractograms of (CrMnFeCoNi)N films grown at different magnetic fields. Peaks marked with * indicate the 200 and 400 reflections from the substrate. (b) FWHM of film 200 peak obtained from peak fitting.

The two peaks may correspond to the crystallographic or growth domains in the films. A more detailed analysis of the FWHM is provided in Fig. S2 in the supplementary material.⁴⁸ When the magnetic field is increased the intensity of peak 2 increases and the FWHM reduces indicating a decrease in the mosaicity within the domain. The peak position of “peak 2” also shifts toward peak 1. The tilt between the domains is approximately 4° for the film grown without magnetic field assistance. As the magnetic field is applied and increased progressively for each deposition, the separation is reduced to approximately 2°. Seeing that the film grown at 8.5 mT displayed the least mosaicity, this film was chosen for further studies.

Figure 3 shows the RSM of the 8.5 mT grown film. Figures 3(a) and 3(b) were obtained at an azimuthal angle, $\phi = 0^\circ$ around the 002 symmetric and 024 asymmetric reciprocal lattice points, respectively. Figures 3(c) and 3(d) are the RSM obtained at $\phi = 90^\circ$. The RSM was measured by aligning the substrate peak position at a position close to 0 in q_y and q_x .

Both RSMs obtained in symmetrical and asymmetrical configuration show the presence of two distinct diffraction spots corresponding to the substrate MgO and the Cantor nitride film. The MgO c lattice parameter obtained from the 002 reflections was $4.222 \pm 0.002 \text{ \AA}$ and the a lattice parameter obtained from the 204 reflections was $4.216 \pm 0.002 \text{ \AA}$. In the case of the film, the c lattice parameter = $3.972 \pm 0.002 \text{ \AA}$, was estimated from the RMS obtained from the 002 reflections in symmetrical configuration at $\phi = 0^\circ$. The a lattice parameter = $4.087 \pm 0.002 \text{ \AA}$ was estimated from the 204 reflection in asymmetric geometry at $\phi = 0^\circ$. The relaxed lattice parameter was calculated to be $4.046 \pm 0.002 \text{ \AA}$. The appearance of distinct diffraction spots on the RSM indicates a degree of epitaxial growth of the Cantor nitride film with cube-on-cube growth $(001)_{\text{film}} \parallel (001)_{\text{MgO}}$, $[100]_{\text{film}} \parallel [100]_{\text{MgO}}$. The in-plane domain size was calculated to be between 40 and 50 nm while the out-of-plane domain sizes were between 95 and 130 nm.

At $\phi = 90^\circ$, the two diffraction spots again correspond to reflections from the MgO substrate and the film [Figs. 3(c) and 3(d)]. From Fig. 3(c), the film diffraction spots at $\phi = 90^\circ$ are different from those at $\phi = 0^\circ$. Here, we observe two peaks suggesting the presence of two crystallographic or growth domains with a tilt in respect to the surface normal [MgO (001) plane]. This is also confirmed in the asymmetrical RSM [Fig. 3(d)], where the tilt is observed and the presence of two peaks within the film diffraction spot.

Figure 4 shows SEM micrographs depicting film surface morphology of the Cantor nitride films grown with varied magnetic field from 0 to 8.5 mT. The films grown without the ion-assistance [0 mT, Fig. 1(a)] contains agglomerated grains/domains. As the magnetic field was increased, the number of these agglomerates progressively decreased leading to a smoother morphology in the case of the film grown with a magnetic field of 8.5 mT. No correlation between the size of the agglomerates and the magnetic field applied during growth was observed.

The cross-sectional SEM micrograph [Fig. 4(h)] shows that the agglomerates are “V” shaped and originate near the film substrate interface in the case of the film grown at 0 mT. However, for the film grown at 8.5 mT, the number of “V” shaped domains is reduced. Moreover, they originate from a specific thickness (approximately 100 nm) of the film and proceed to enlarge as the film thickness increases. This depth at which the grain starts to grow corresponds to the out-of-plane domain size of the epitaxial layer (95–130 nm) determined from the RSM (Fig. 2).

Figure 5 shows the (S)/(HR)TEM images of the Cantor nitride thin films grown with a magnetic field strength of 8.5 mT. Figure 5(a) shows the cross-sectional STEM image. The film appears visually dense with the presence of two different regions identifiable from the contrast differences. From the inset selected area diffraction pattern (SAED) pattern [Figs. 5(a) and 5(i)] taken

12 February 2024 15:01:40

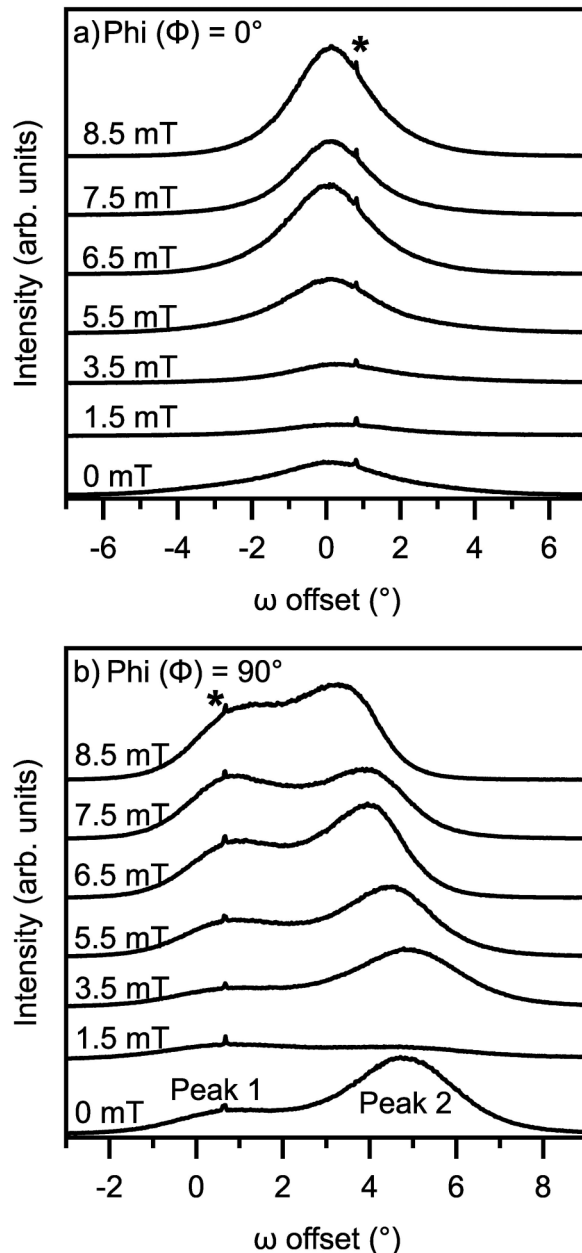


FIG. 2. (a) Rocking curves of Cantor nitride (002) reflection obtained at an azimuthal angle (ϕ) = 0° and (b) $\phi = 90^\circ$.

closer to the top of the coating (darker contrast), we observe that the film displays a 200 texture along the growth direction. The epitaxial region could only be observed in the beginning stages of films growth and is seen in lighter contrast in comparison to the rest of the film. The area below the dashed line in Fig. 5(a) corresponds to the epitaxial region while the area above the dashed line corresponds to the textured region. The lattice parameter along the

growth direction of the textured region was found to be the same as the epitaxial region of the film. HRTEM images were acquired from the region marked below the dashed line and are shown in Fig. 5(b). The images along with the inset corresponding fast Fourier transforms (FFTs) provide further proof of epitaxy in the first 80–100 nm of growth [Fig. 5(b)(i) and (ii)].

Above 100 nm, the growth and orientation of the grains in the films differed. Figure 5(c) provides a localized view at the top 100 nm of the film surface where the presence of a “V” shaped agglomerate is observed. The change in in-plane orientation along with the 2° tilt in domains with respect to surface normal can be observed in the inset FFT’s [Fig. 5(c)(i) and (ii)].

For complementary analysis and on the best quality sample, BLS was performed on the Cantor nitride film grown at 8.5 mT. Figure 6 shows the BLS spectrum of the Cantor nitride film grown at 8.5 mT obtained for two different directions of propagation of SAW along the film plane, $[100]_{\text{MgO}}$. We measured the Rayleigh wave sound velocity of (CoCrMnFeNi)N film $V_{\text{R}[100]} = 3014 \pm 5$ m/s. The retrieved elastic constants from fitting of BLS spectra were $C_{11} = 320$ GPa, $C_{12} = 125$ GPa, and $C_{44} = 66$ GPa. We calculated polycrystalline Young’s modulus $E = 204$ GPa and Poisson’s ratio of the Cantor nitride $\nu = 0.321$. These values are not only in line with Young’s modulus and Poisson’s ratio of bulk steel and α -iron but also with similar Cantor alloy-based thin films.^{3,4,39–41}

IV. DISCUSSION

(CrMnFeCoNi)N epitaxial films were grown by low temperature, magnetic-field-assisted magnetron sputtering. As the magnetic field was increased from 0 to 8.5 mT, the ion flux reaching the substrate also increased from $\sim 1.5 \times 10^{14}$ to $9 \times 10^{14} \text{ cm}^{-2} \text{ s}^{-1}$, and the ion-to-metal flux ratio from ~ 0.3 to 1.8. The ion energy remained constant at ~ 20 eV.

Following previous studies on a similar material system, the films displayed the predicted NaCl B1 structure.⁴² The x-ray diffractograms of the films indicate a 002 highly oriented growth while the rocking curves obtained at $\phi = 0^\circ$ display a reducing mosaicity as the ion flux was increased. No noticeable changes in composition were observed with the increasing ion flux during growth (Fig. 1 and Table II). The density of the films was, however, seen to increase from 6.20 to 6.72 g/cm³ with increasing ion flux. Similar features have been observed in experimental studies on the TiN binary nitride system when low-energy ion-irradiation reduces porosity in the films.²⁸ Theoretical molecular dynamic simulations of Ni films subjected to 100 eV Ar-ion bombardment during growth have been able to provide an explanation for the densification. The study suggested that the protruding ledges that form during growth can be broken down through ion bombardment, thereby avoiding shadowing and void formation leading to dense films.²⁴

The evidence of epitaxial growth was confirmed in the RMS of the film grown with highest ion flux (8.5 mT magnetic field). Further proof of epitaxial growth was seen in the HRTEM image and inset FFTs [Fig. 5(b)]. The film displayed a cube-on-cube relationship with the substrate. This type of growth is not surprising considering that the substrate, which acts as a template has a lattice parameter close to that of the Cantor nitride itself (4.21 Å). Similar

12 February 2024 15:01:40

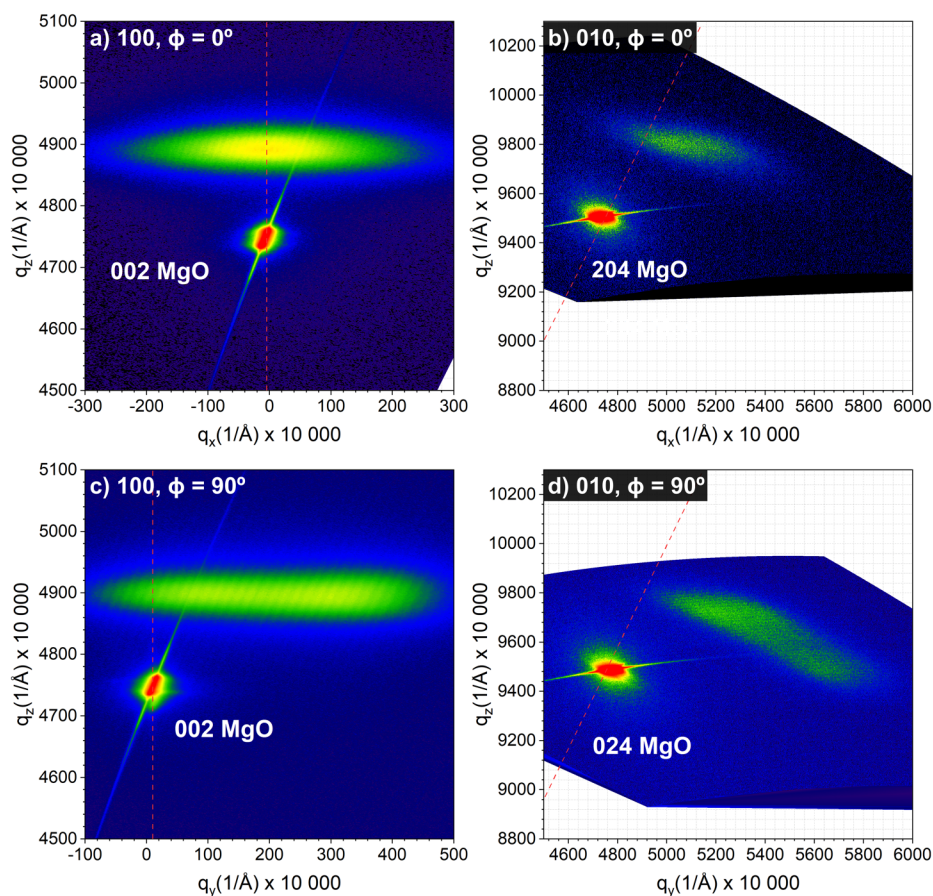


FIG. 3. RSM of Cantor nitride films grown at 8.5 mT depicting epitaxial growth. (a) 002 symmetric RSM and (b) 024 asymmetric acquired at $\phi = 0^\circ$. (c) 002 symmetric RSM and (d) 024 asymmetric acquired at $\phi = 90^\circ$.

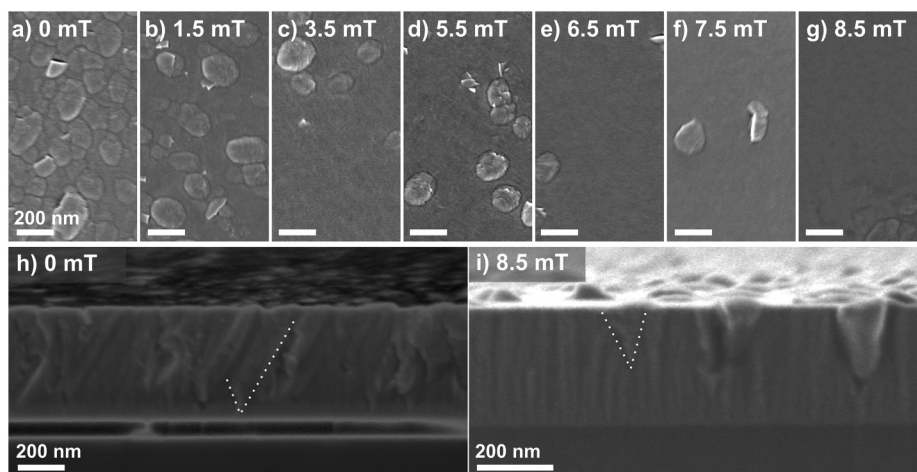


FIG. 4. (a)–(g) SEM images showing the planar view of Cantor nitride films grown with different magnetic fields. (h) and (i) Cross-sectional SEM micrograph of film grown at 0 and 8.5 mT, respectively.

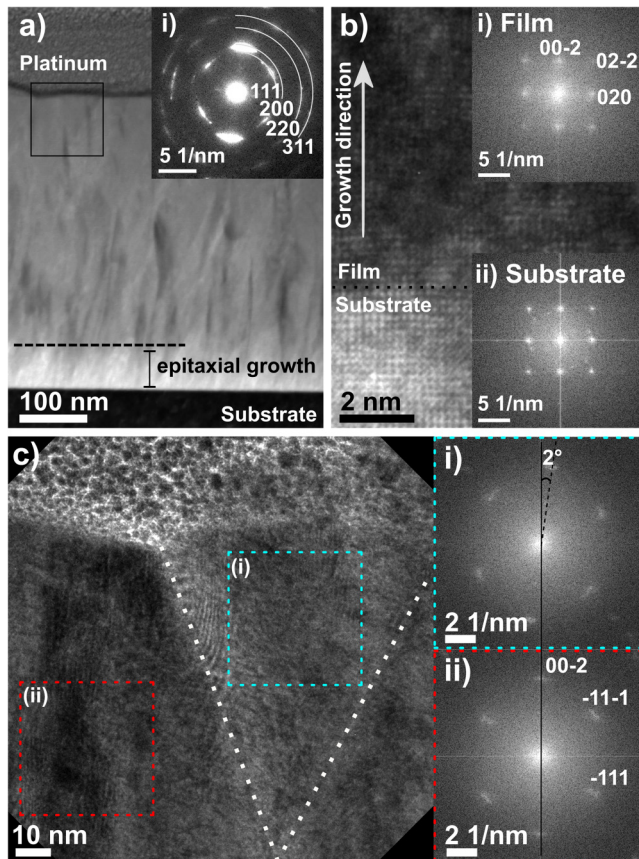


FIG. 5. (a) STEM cross-sectional image of Cantor nitride thin film grown at 8.5 mT magnetic field. (i) Inset SAED from film cross section. (b) HRTEM of substrate-film interface with inset FFTs from the (i) film and (ii) substrate depicting epitaxial growth of the film. (c) HRTEM of region marked within the black square in Fig. 5(a) indicating the two domains along with corresponding FFTs regions marked within squares (i) and (ii).

growth has been observed in the case of the metallic Cantor films along with binary nitride thin films on MgO substrates.^{8,15,43–45}

At a different azimuth angle ($\phi = 90^\circ$), two crystallographic domains with a tilt in growth were present. The domain corresponding to peak 1 in Fig. 2(b) has a tilt of approximately 1° with respect to the surface normal drawn from the substrate. The tilt of this domain was found to remain constant with the variation of the magnetic field. The domain corresponding to peak 2 in Fig. 2(b), on the other hand, had a much larger tilt of approximately 4° . This tilt was, however, seen to be reduced as the magnetic field was increased from 0 to 8.5 mT. The tilted “V” shaped grain, which was observable on the HRTEM images, appeared once the epitaxial growth was broken and where the textured growth began. The tilt in growth could be a consequence of the deposition geometry and the absence of substrate rotation during deposition. It could also be due to the presence of imperfections or steps in the MgO substrate, which could also lead to 2D island nucleation during epitaxial-step flow growth.⁴⁶

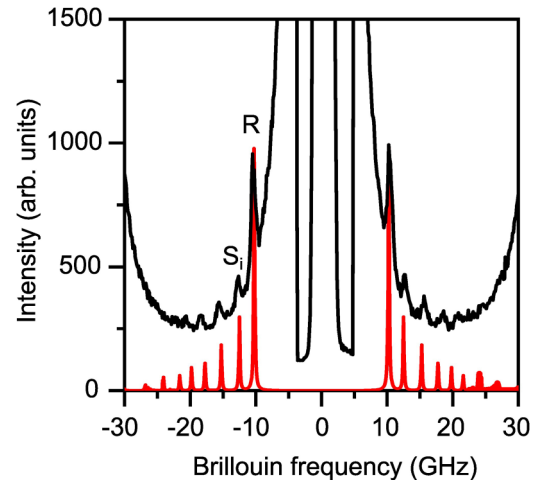


FIG. 6. Brillouin spectrum for an angle of incidence of 65° and propagation direction along [100] in the MgO(001) plane. R_i and S_i denote the Rayleigh and Sezawa surface waves, respectively. Below in is the power spectrum $\langle u_z^2(z=0, f) \rangle$ of the vertical displacement at the free surface.

From the SEM analysis of the films, the presence of imperfection along the film cross section was observed [Fig. 4(h)]. The growth of the “V” shaped agglomerates, or crystals, was seen to be initiated at the substrate for the film grown with the least ion flux (0 mT). As the ion flux was increased, the number of agglomerates reduced, and their origination started much later in the film [Fig. 4(i)]. From the HRTEM image and corresponding FFTs in Fig. 5(c), we can say that these “V” shaped agglomerates correspond to the secondary domain tilted (2° – 4°) observed in the rocking curves and the RSM obtained at $\phi = 90^\circ$.

There are several possibilities for the presence and growth of this second domain. The first possible origin is related to the stress level generated during growth. The lattice parameter of MgO (100) is 4.21 \AA . The calculated a and c lattice parameters of the Cantor nitride film grown in high magnetic field/ion flux conditions were found to be 4.08 and 3.98 \AA , respectively. A difference of 2% is seen between a and c implying that in the deposited film, the lattice is not a perfect cube. Moreover, the difference in lattice parameter between the substrate and film is approximately +3%. Therefore, the film would be under a tensile stress for epitaxial growth. The epitaxy can be broken after a certain thickness in an attempt to release the stresses in the film, which in the present case happened at different thickness. Without magnetic field assistance (0 mT), the films grow with a lower epitaxial quality and numerous domains. As the ion flux is increased, the higher number of low-energy ions provide enough kinetic energy for enhancing epitaxial growth. Ar-ion bombardment aids in maintaining epitaxial growth and hampers the nucleation of the secondary domain.

A possible solution to improving and extending the epitaxial region could be by bombarding the film with not only higher flux of ions but higher energy ions as well, as seen in the case of (CrFeCoNi)N films where higher energy Ar-ion bombardment at 300°C results in improved crystal quality.^{22,47}

12 February 2024 15:01:40

V. CONCLUSIONS

Epitaxial Cantor nitride thin films were successfully grown by magnetic-field-assisted magnetron sputtering. This technique was employed to substitute the contributions of thermal energy on the growing films by kinetic energy. A solenoid coil placed around the substrate holder was able to produce a magnetic field from 1.5 to 8.5 mT. This resulted in an increase in the ion flux at the substrate from $\sim 1.5 \times 10^{14}$ to $9 \times 10^{14} \text{ cm}^{-2} \text{ s}^{-1}$.

The films which were grown on MgO (100) substrates displayed an NaCl B1 structure. The film grown without the magnetic field assistance was seen to be highly textured in nature. As the magnetic field increased, cube-on-cube, epitaxial growth was promoted. The reciprocal space maps indicated the presence of two domains with a 2° – 4° tilt with respect to the surface normal. The domains could be a result of stress relaxation in the films after a threshold-thickness ~ 80 – 100 nm .

The single crystal elastic constants of the film were measured by BLS, $C_{11} = 320 \text{ GPa}$, $C_{12} = 125 \text{ GPa}$, and $C_{44} = 66 \text{ GPa}$. The calculated polycrystalline Young's modulus (204.01 GPa) and Poisson's ratio (0.3210) were found to be in line with available experimental data of bulk polycrystalline materials and theoretical ones calculated by *ab initio* methods.

In this study, we have demonstrated that the Cantor nitride can be grown epitaxially. The quality of epitaxy was limited to a certain thickness after which textured films were grown. Ion bombardment may during growth play an important role leading to larger grains and better epitaxy. The study lays the foundation for future work concerning the modeling of multicomponent systems for a better understanding of the material system.

ACKNOWLEDGMENTS

The work was supported financially by the VINNOVA Competence Centre FunMat-II (Grant No. 2016-05156), the Swedish Government Strategic Research Area in Materials Science on Functional Materials at Linköping University (Faculty Grant SFO-Mat-LiU No. 2009 00971), the Knut and Alice Wallenberg foundation through the Wallenberg Academy Fellows program (No. KAW-2020.0196), and the Swedish Research Council (VR) under Project No. 2021-03826. Support of accelerator operation at Uppsala University by the Swedish Research Council VR-RFI under Contract No. 2019_00191 is gratefully acknowledged.

AUTHOR DECLARATIONS

Conflict of Interest

The authors have no conflicts to disclose.

Author Contributions

Smita G. Rao: Conceptualization (equal); Data curation (equal); Formal analysis (lead); Investigation (lead); Writing – original draft (lead); Writing – review & editing (equal). **Pascal Manuel Illgner:** Data curation (equal); Formal analysis (supporting); Writing – review & editing (supporting). **Robert Boyd:** Data curation (equal); Formal analysis (equal); Investigation (equal); Writing – review & editing (supporting). **Gyula Nagy:** Data curation (equal); Formal

analysis (equal); Investigation (equal); Writing – review & editing (supporting). **Philippe Djemia:** Data curation (equal); Formal analysis (equal); Writing – review & editing (supporting). **Daniel Primetzhofer:** Conceptualization (equal); Formal analysis (supporting); Investigation (supporting); Writing – review & editing (supporting). **Ivan Petrov:** Conceptualization (equal); Formal analysis (equal); Investigation (equal); Methodology (equal); Writing – review & editing (equal). **Arnaud le Febvrier:** Conceptualization (equal); Formal analysis (equal); Supervision (equal); Validation (equal); Writing – review & editing (equal). **Per Eklund:** Conceptualization (equal); Funding acquisition (equal); Investigation (equal); Supervision (equal); Validation (equal); Writing – review & editing (equal).

DATA AVAILABILITY

The data that support the findings of this study are available from the corresponding author upon reasonable request.

REFERENCES

- B. Cantor, *Mater. Sci.* **120**, 100754 (2021).
- Z. Zeng *et al.*, *J. Mater. Res. Technol.* **15**, 1920 (2021).
- G. Laplanche, P. Gadaud, O. Horst, F. Otto, G. Eggeler, and E. P. George, *J. Alloys Compd.* **623**, 348 (2015).
- G. Laplanche, P. Gadaud, C. Bärsch, K. Demtröder, C. Reinhart, J. Schreuer, and E. P. George, *J. Alloys Compd.* **746**, 244 (2018).
- N. E. Koval, J. I. Juaristi, R. Díez Muiño, and M. Alducin, *J. Appl. Phys.* **127**, 145102 (2020).
- E. Lewin, *J. Appl. Phys.* **127**, 160901 (2020).
- G. Radnóczy, R. Dedoncker, G. Z. Radnóczy, Z. Czirány, A. Sulyok, V. Kovács-Kis, and D. Depla, *Surf. Coat. Technol.* **421**, 127433 (2021).
- G. Abadias, C.-H. Li, L. Belliard, Q. M. Hu, N. Greneche, and P. Djemia, *Acta Mater.* **184**, 254 (2020).
- L. Hultman, C. Engström, and M. Odén, *Surf. Coat. Technol.* **133–134**, 227 (2000).
- J.-E. Sundgren, "Formation and characterization of titanium nitride and titanium carbide films prepared by reactive sputtering," Department of Physics and Measurement Technology, Linköping University, 1982, see https://inis.iaea.org/search/search.aspx?orig_q=RN:13693374 (last accessed January 18, 2023).
- L. Hultman, *Vacuum* **57**, 1 (2000).
- N. Koutná, L. Löfler, D. Holec, Z. Chen, Z. Zhang, L. Hultman, P. H. Mayrhofer, and D. G. Sangiovanni, *Acta Mater.* **229**, 117809 (2022).
- D. G. Sangiovanni, B. Alling, P. Steneteg, L. Hultman, and I. A. Abrikosov, *Phys. Rev. B* **91**, 54301 (2015).
- K. M. Calamba, J. Salamaia, M. P. J. Jösaar, L. J. S. Johnson, R. Boyd, J. F. Pierson, M. A. Sortica, D. Primetzhofer, and M. Odén, *Acta Mater.* **203**, 116509 (2021).
- J. Salamaia *et al.*, *Mater. Des.* **224**, 111327 (2022).
- U. Helmersson, S. Todorova, S. A. Barnett, J.-E. Sundgren, L. C. Markert, and J. E. Greene, *J. Appl. Phys.* **62**, 481 (1987).
- D. Gall, I. Petrov, N. Hellgren, L. Hultman, J. E. Sundgren, and J. E. Greene, *J. Appl. Phys.* **84**, 6034 (1998).
- J. E. Greene, *Crit. Rev. Solid State Mater. Sci.* **11**, 189 (1983).
- S. G. Rao *et al.*, *Phys. Rev. Mater.* **7**, 055002 (2023).
- M. M. S. Villamayor, J. Keraudy, T. Shimizu, R. P. B. Vilão, R. Boyd, D. Lundin, J. E. Greene, I. Petrov, and U. Helmersson, *J. Vac. Sci. Technol. A* **36**, 061511 (2018).
- T. Lee, H. Seo, H. Hwang, B. Howe, S. Kodambaka, J. E. Greene, and I. Petrov, *Thin Solid Films* **518**, 5169 (2010).
- S. G. Rao, R. Shu, R. Boyd, A. le Febvrier, and P. Eklund, *Vacuum* **204**, 111331 (2022).

- ²³U. Helmersson, M. Lattemann, J. Bohlmark, A. P. Ehiasarian, and J. T. Gudmundsson, *Thin Solid Films* **513**, 1 (2006).
- ²⁴T. Itoh, *Ion Beam Assisted Film Growth* (Elsevier, 2012), see <https://books.google.se/books?id=TTvixGiSggwC>.
- ²⁵L. Hultman, J. E. Sundgren, J. E. Greene, D. B. Bergstrom, and I. Petrov, *J. Appl. Phys.* **78**, 5395 (1995).
- ²⁶C. Engström, T. Berlind, J. Birch, L. Hultman, I. P. Ivanov, S. R. Kirkpatrick, and S. Rohde, *Vacuum* **56**, 107 (2000).
- ²⁷I. Ivanov, P. Kazansky, L. Hultman, I. Petrov, and J-E Sundgren, *J. Vac. Sci. Technol. A* **12**, 314 (1994).
- ²⁸I. Petrov, L. Hultman, U. Helmersson, J. E. Sundgren, and J. E. Greene, *Thin Solid Films* **169**, 299 (1989).
- ²⁹A. Le Febvrier, J. Jensen, and P. Eklund, *J. Vac. Sci. Technol. A* **35**, 021407 (2017).
- ³⁰A. le Febvrier, L. Landälv, T. Liersch, D. Sandmark, P. Sandström, and P. Eklund, *Vacuum* **187**, 110137 (2021).
- ³¹I. Petrov, V. Orlinov, I. Ivanov, and J. Kourtev, *Plasma Phys.* **28**, 157 (1988).
- ³²P. Ström and D. Primetzhof, *J. Instrum.* **17**, P04011 (2022).
- ³³J. L. Campbell, D. J. T. Cureatz, E. L. Flannigan, C. M. Heirwegh, J. A. Maxwell, J. L. Russell, and S. M. Taylor, *Nucl. Instrum. Methods Phys. Res., Sect. B* **499**, 77 (2021).
- ³⁴M. Mayer, *SIMNRA User's Guide*, Report IPP 9/113 (Max-Planck-Institut für Plasmaphysik, Garching, Germany, 1997).
- ³⁵G. Abadias, P. Djemia, and L. Belliard, *Surf. Coat. Technol.* **257**, 129 (2014).
- ³⁶L.-F. Zhu *et al.*, *J. Mech. Behav. Biomed. Mater.* **20**, 296 (2013).
- ³⁷M. Friák, W. A. Counts, D. Ma, B. Sander, D. Holec, D. Raabe, and J. Neugebauer, *Materials* **5**, 1853 (2012).
- ³⁸H. Titrian, U. Aydin, M. Friák, D. Ma, D. Raabe, and J. Neugebauer, *MRS Proc.* **1524**, 301 (2013).
- ³⁹H. F. Zhang, H. L. Yan, H. Yu, Z. W. Ji, Q. M. Hu, and N. Jia, *J. Mater. Sci. Technol.* **48**, 146 (2020).
- ⁴⁰S. A. Kim and W. L. Johnson, *Mater. Sci. Eng. A* **452-453**, 633 (2007).
- ⁴¹R. Dedoncker, P. Djemia, G. Radnóczy, F. Tétard, L. Belliard, G. Abadias, N. Martin, and D. Depla, *J. Alloys Compd.* **769**, 881 (2018).
- ⁴²S. G. Rao *et al.*, "Phase formation in CrFeCoNi nitride thin films," *arXiv2211.05471* (2022).
- ⁴³A. B. Mei, B. M. Howe, C. Zhang, M. Sardela, J. N. Eckstein, L. Hultman, A. Rockett, I. Petrov, and J. E. Greene, *J. Vac. Sci. Technol. A* **31**, 061516 (2013).
- ⁴⁴C.-S. Shin, Y.-W. Kim, N. Hellgren, D. Gall, I. Petrov, and J. E. Greene, *J. Vac. Sci. Technol. A* **20**, 2007 (2002).
- ⁴⁵H. Schwarz *et al.*, "Fabrication of single-crystalline CoCrFeNi thin films by DC magnetron sputtering: A route to surface studies of high-entropy alloys," *Adv. Mater.* (published online) (2023).
- ⁴⁶G. S. Bales and A. Zangwill, *Phys. Rev. B* **41**, 5500 (1990).
- ⁴⁷M. Marinov, *Thin Solid Films* **46**, 267 (1977).
- ⁴⁸See supplementary material online for plasma characterization details, detailed XRD rocking curve measurements for the films series, and the oxygen content and density determined by RBS.